Journal of Atmospheric Chemistry 7 (1988) 153–176.

Measuring Correlations Between Atmospheric Oxygen and Carbon Dioxide Mole Fractions: A Preliminary Study in Urban Air

RALPH F. KEELING
Harvard University, E.S.L. 40 Oxford St., Cambridge, MA 02138, U.S.A.

(Received: 27 October 1987; revised: 9 February 1988)

Abstract. On 25 and 26 October 1986 the air in Cambridge, Massachusetts was monitored for O_2 and CO_2 mole fraction. O_2 concentrations were detected from changes in the relative refractivity of dried air between two lines of ^{198}Hg at 2537.269 and 4359.562 Å using dual-wavelength interferometry. Changes in oxygen mole fraction were resolved with two-minute time resolution to a precision of ±2.0 ppm. Changes in O_2 were shown to be strongly anticorrelated with changes in CO_2 as expected for combustion processes. The demonstrated instrumental capabilities are appropriate for measuring changes in O_2 mole fraction in background air which could be of importance to a broad range of biogeochemical studies.

Key words. Atmospheric oxygen, atmospheric carbon dioxide, carbon cycle, urban air, interferometry.

1. Introduction

It is well known that photosynthesis, respiration, and the burning of fuels cause variations in the abundance of atmospheric carbon dioxide. It has been generally overlooked, however, that these same processes must alter the proportion of atmospheric oxygen relative to nitrogen and the inert gases. Since the landmark study of Benedict (1912) showed conclusively that atmospheric O_2 was constant to a high level, only a few measurements of the atmospheric O_2 fraction have been reported (Krogh, 1919; Carpenter, 1937; Lockhart and Court, 1942; Shepherd, 1935; Hughes, 1968; Machta and Hughes, 1970). Except for the study of Lockhart and Court (1942), whose results have been questioned by Machta and Hughes (1970) and by Glueckauf (1951), no studies have reported measurements which resolve changes in background air.

The paucity of data for atmospheric oxygen mole fraction reflects the difficulty of making these measurements. Oxygen comprises 20.946 mole % of dry air (Machta and Hughes, 1970) which makes it about 600 times more abundant than carbon dioxide. Secular and seasonal changes in O_2 mole fraction are expected at approximately the same absolute levels as have been observed for CO_2, i.e. at the 0.0001 to 0.001 mole % level (throughout the remainder of this paper, changes in O_2 are expressed in units of parts per million (ppm)

where 1 ppm = 0.0001 mole % and where the O_2 mole % is expressed relative to sum of N_2, O_2, and the inert gases). Neither the traditional technique of chemically extracting the O_2 and measuring the weight or volume change nor the more recent technique employing paramagnetic analyzers (Machta and Hughes, 1970) are sufficiently precise to resolve such small changes.

Direct measurements of changes in atmospheric oxygen mole fraction would substantially improve the framework for studying the carbon cycle and the perturbations due to human activities. Specifically, measurements of seasonal changes in atmospheric oxygen mole fraction would constrain estimates of the seasonal fluxes of O_2 from the land biosphere and from the air-sea interface. This would improve the basis for estimating both terrestrial and marine productivities. Detecting the presumed long-term depletion of atmospheric O_2 would constrain estimates of the total CO_2 source from burning fossil fuel and oxidation of biomatter. This would provide an objective constraint on models of the uptake of CO_2 by the ocean which are needed to forecast future CO_2 levels and future climate. In a broader sense, atmospheric O_2 is a major trace of global biological activity which could be exploited to understand processes occurring over a wide range of temporal and spatial scales.

This paper introduces a new technique for measuring changes in atmospheric O_2 mole fraction based on resolving small changes in the optical dispersion of air. The biogeochemical significance of such measurements is discussed further in the following section. The physical basis and implementation of this technique are described in Section 3. Results for a preliminary study of O_2 and CO_2 mole fractions in urban air are described in Section 4.

2. What Can Be Learned From Measurements of Atmospheric Oxygen Mole Fraction?

Sources and sinks of atmospheric O_2 and CO_2 are stoichiometrically linked through the oxidation and reduction of organic matter: i.e. through photosynthesis and respiration

$$CO_2 + H_2O \rightleftharpoons H_2CO + O_2, \tag{1}$$

where CH_2O represents the approximate composition of biomatter, and through the burning of fuels

$$CH_x + (1 + \frac{1}{4}x)O_2 \rightarrow CO_2 + \frac{1}{2}xH_2O. \tag{2}$$

For such redox reactions a net sink of O_2 corresponds to net source of CO_2 and vice versa. The ratio of the change in O_2 and CO_2 depends on the oxidation state of the organic material. Oxidation states are often described in terms of the reduction level – i.e. the ratio of moles O_2 consumed per mole CO_2 produced upon complete combustion (Giese, 1973, pp. 446). For example, the reduction

level of carbohydrates is 1.0, whereas the reduction level of methane is 2.0.

Both atmospheric O_2 and CO_2 are also significantly influenced by interactions with seawater. There are significant difference between the capacitative and kinetic factors governing the storage of O_2 and CO_2 in seawater and exchange of O_2 and CO_2 across the air-sea interface. The differences are principally due to the reaction of dissolved CO_2 with seawater to form carbonic acid, and bicarbonate and carbonate ions. Thus the effective solubility of CO_2 in seawater is much greater than the solubility of O_2. An effective solubility coefficient for CO_2 (C_{eff}) can be defined by the ratio of the change in dissolved inorganic carbon (DIC) to the change in the partial pressure P_{CO_4} of CO_2 (P_{CO_2}) at equilibrium

$$C_{\text{eff}} = \frac{\mathrm{d}DIC}{\mathrm{d}P_{CO_2}} = R^{-1} \cdot \frac{DIC}{P_{CO_2}}, \tag{3}$$

where R is the Revelle Factor (see e.g. Broecker *et al.*, 1979). For example, in 24 °C water in the Western Pacific, we have $R = 9$, $DIC = 1950$ μ mole kg^{-1}, and $P_{CO_2} = 3.4 \times 10^{-4}$ atm (Broecker and Peng, 1982, pp. 157–159) which yields an effective solubility coefficient of 6.4×10^5 μ mole kg^{-1} atm^{-1}. This is six hundred times greater than the solubility coefficient of O_2 in 24 °C water of 1.03×10^3 μ mole kg^{-1} atm^{-1} (Broecker and Peng, 1982, p. 112). Likewise, the rate at which surface waters come into equilibrium with the atmosphere, is roughly twenty times slower for CO_2 than O_2 (Broecker and Peng, 1982, p. 155; Peng *et al.*, 1987). CO_2 is exchanged slowly because the predominant species of DIC in sea water are carbonate and bicarbonate which do not directly influence the CO_2 partial pressure.

The most pronounced features seen in records of atmospheric CO_2 mole fraction are a regular seasonal variation caused primarily by seasonal exchange with the land biosphere and a long-term increase caused primarily by burning fossil fuel (Keeling *et al.*, 1982; Kohmyr *et al.*, 1985). The close link between oxidative sources and sinks of O_2 and CO_2 implies that there must exist corresponding variations in the atmospheric O_2 fraction. Primarily because interactions with sea-water are also important, however, the variation in atmospheric O_2 is not uniquely determined by the variation in CO_2. Therefore, measurements of atmospheric O_2 mole fraction on these time scales would provide important new constraints on the global carbon cycle.

Measurements of seasonal variations in atmospheric O_2 mole fraction would constrain the magnitude of marine biological new production – i.e., the amount of carbon which is photosynthetically fixed and subsequently exported from the euphotic zone. The magnitude of new production is important because it is closely tied to the rates of cycling of nutrients and many trace chemicals in the ocean. Recently, there has been considerable debate over the magnitude of new production. Bottle incubations which measure rates of ^{14}C and ^{15}N assimilation lead to estimates of new production of approximately 1 mole m^{-2} yr^{-1} in the

central gyres (Eppley and Peterson, 1979). This type of estimate has been challenged by researchers who have examined the cycling of oxygen in the mixed layer and upper thermocline (Shulenberger and Reid, 1981; Jenkins, 1983; Jenkins and Goldman, 1985). The oxygen studies lead to estimates of new production of approximately 5 mole C m^{-2} yr^{-1}. The oxygen data have raised serious questions concerning the validity of incubation studies, but the oxygen studies have not gone unchallenged (Platt, 1984). One particular difficulty is the need to interpret the change in dissolved oxygen in terms of *in situ* production without any firm data for the fluxes of oxygen across the air-sea interface.

With ppm-level oxygen measurement capability, it would be possible to estimate the net air-sea exchange of O_2, not by measuring changes in dissolved O_2, but by detecting corresponding changes in the atmospheric O_2 reservoir. Jenkins and Goldman (1985) estimate the magnitude of the seasonal air-sea flux of O_2 induced by biology in the Sargasso sea is of the order of 5 moles m^{-2}. Fluxes of this magnitude, if typical of the major ocean basins poleward of 20° (where significant seasonal fluxes are expected) imply variations in the atmospheric O_2 mole fraction of 4 to 8 ppm over a hemispheric scale. Even larger variations would be expected in proximity to high productivity regions of the oceans.

In general, it is expected that seasonal air-sea exchange of O_2 should be larger (in moles) than seasonal exchange of CO_2. Firstly, while the time-scale for the mixed layer to equilibrate with the atmosphere is a few weeks for O_2, it is a year or so for CO_2 (Broecker and Peng, 1982, p. 155). This implies that short-term processes such as plankton blooms, the seasonal warming and cooling of surface waters, or the rapid weakening of the seasonal thermocline in winter – all of which initially produce comparable surface saturation anomalies in oxygen and total inorganic carbon on a moles/kg basis – are expected to drive a larger flux of O_2 across the air-sea interface than the flux of CO_2. Secondly, while the biological and thermal driving forces for seasonal air-sea exchange of CO_2 tend to oppose each other (biology drives ingassing flux of CO_2 in spring and summer when temperature is driving outgassing flux), the biological and thermal driving forces for seasonal air-sea exchange of O_2 tend to reinforce each other (both driving outgassing in spring and summer) (Peng *et al.*, 1987).

The interpretation of the seasonal variations in O_2 mole fraction in terms of air-sea exchange of O_2 will be complicated by the need to account for (1) the variations in O_2 caused by photosynthesis and respiration of the land biosphere, (2) the variations in N_2 and Ar caused by seasonal temperature changes in ocean surface waters, and (3) atmospheric mixing. In principle, none of these complications presents serious difficulties. The land-biosphere component to the O_2 variations can be estimated from simultaneous measurements of CO_2 and $^{13}C/^{12}C$ ratios in atmospheric CO_2 since the seasonal variations in CO_2 and especially in $^{13}C/^{12}C$ are strongly influenced by exchange with the land biosphere but only weakly influenced by air-sea exchange (see, e.g., Mook *et al.*,

1983). The residual variation in O_2 mole fraction (the variation remaining after removing the land-biosphere component) could be modeled using an oceanic model to estimate air-sea exchange of O_2, N_2 and the inert gases coupled to a model of the atmospheric motion field. With the air motions constrained by independent tracers, the residual variation would constrain the air-sea exchange fluxes which, in turn, implies direct constraints on estimates of ocean biological productivities. Models of this general character, albeit with simplified treatment of the oceanic processes, have been used for modeling CO_2 seasonal cycles (Fung *et al.*, 1983; Heimann *et al.*, 1986; Pearman and Hyson, 1980). Note that O_2 data from just a few well-chosen locations could provide a new global constraint on marine biological productivity.

A completely different set of questions would be addressed by detecting long-term variations in the O_2 mole fraction. Some time ago, Machta (1980) proposed that measurement of the presumed long-term depletion in O_2 could be used to constrain the magnitude of recent changes in the land biosphere. Burning fossil fuel decreases atmospheric O_2 at a predictable rate. Unlike the corresponding increase in atmospheric CO_2 which drives a substantial flux of CO_2 into the ocean, the decrease in O_2 partial pressure cannot drive a significant flux of O_2 out of the ocean because the oceans' capacity for O_2 is too small: only about 1% of the total O_2 in the ocean-atmosphere system is stored in the ocean (Keeling, 1988, p. 67). On this basis, the long-term changes in atmospheric O_2 should be easier to interpret than long-term changes in CO_2. If the consumption of O_2 from burning fossil fuel were subtracted from the measured loss in atmospheric O_2, the residual O_2 loss would reflect the net O_2 consumed from the oxidation of biomatter. The net source of CO_2 from the biosphere could be directly calculated by dividing the residual O_2 loss by the appropriate reduction level for biospheric carbon (approximately 1.0). The biospheric CO_2 source derived in this way would account for all oxidative processes including global deforestation, soil oxidation, and any changes in net-ecosystem production.

Measuring changes in the size of the land biosphere could provide one of the most valuable indexes of the impact of human activities on global ecology. Today, slash and burn agriculture is causing the rapid destruction of tropical forests. Also, plants are being exosed to increasing levels of toxic chemicals such as ozone (Logan, 1985). At the same time, however, some previously farmed land is being reforested today, and the increase in atmospheric CO_2 and the release of fixed nitrogen from industrial activities may be stimulating an increase in global photosynthesis. We do not know the relative importance of such processes nor do we know their net impact. Because most of these processes are now occurring at an accelerating pace, there is a clear need to develop methods for measuring the changes which are likely to occur over the next few decades.

One particular area where knowledge of the net change in the biosphere is important is in studies of the uptake by the oceans of CO_2 produced by burning fossil fuel and oxidation of biomatter. Burning fossil fuel currently adds about

4×10^{14} moles/yr of CO_2 to the atmosphere (Marland and Rotty, 1984). The observed increase in atmospheric CO_2 (Keeling *et al.*, 1982; Neftel *et al.*, 1985) acounts for approximately one half of all the fossil-fuel CO_2 added to the atmosphere. Presumably most of the remaining CO_2 has entered the ocean (see, e.g., Broecker *et al.*, 1979). Oceanographers have found that their models of ocean vertical transport and air-sea exchange can account for the observed rise in CO_2 only if they assume that the land biosphere has recently been near steady state: current ocean models require the recent biospheric net source to be from -0.8×10^{14} to $+0.8 \times 10^{14}$ moles/yr (Siegenthaler and Oeschger, 1987; Enting and Pearman, 1987). In contrast, terrestrial ecologists, working from estimates of changes in carbon storage on land, estimate that the land biosphere is a net source of 0.8×10^{14} to 2.2×10^{14} moles/year (Houghton *et al.*, 1987; Olson, 1982). The apparent discrepancy between the estimates of the oceanographers and ecologists sheds serious doubt on our understanding of the carbon cycle as a whole, and more specifically, makes it impossible to validate models of oceanic CO_2 uptake which are needed to forecast future atmospheric CO_2 levels and thus future climatic conditions.

The long-term change in atmospheric O_2 mole fraction X_{O_2} can be estimated according to

$$\delta X_{O_2} = (1 - X_{O_2}) \frac{\delta M_{O_2}}{M_{air}} \tag{4}$$

where M_{air} is the total number of moles of N_2, O_2, and the inert gases, and M_{O_2} is the total number of moles of O_2. Because sources and sinks of atmospheric N_2 (Söderlund and Svensson, 1976) are at least ten times smaller than sources and sinks of O_2, and because atmospheric N_2 is four times more abundant than O_2, the long-term changes in N_2 are negligible in the present context. The current change in oxygen mole fraction due to the land biosphere is estimated to be –0.4 to –1.0 ppm/yr. This estimate is based on assuming the land biosphere is a source of 0.8×10^{14} to 2.2×10^{14} moles C/yr as suggested by the study by Houghton *et al.* (1987), assuming the appropriate reduction level for land-biosphere carbon is 1.05 (Keeling, 1988, pp. 100–103), and approximating M_{air} by the total mass of dry air of 5.123×10^{18} kg (Trenberth *et al.*, 1987) or 1.768×10^{20} moles. The biospheric component is superimposed on the O_2 loss due to burning fossil fuel estimated for 1980 as 6.1×10^{14} moles/yr (Keeling, 1988, p. 97) or –2.7 ppm/yr. The globally averaged long-term change in O_2 could be detected by measurements conducted at just a few stations because the lower atmosphere (troposphere) is mixed on a time scale of less than two years.

One limitation to estimating changes in the land biosphere from atmospheric O_2 data is that secular changes in cycling of nutrients in the oceans conceivably could be causing the oceans to be a significant long-term source or sink of O_2. Peng and Broecker (1984) recently considered three scenarios for recent changes in nutrient cycles, and the argue that significant changes in atmospheric CO_2

cannot have been caused by any plausible variations in nutrient cycles over the past century. Presumably changes in atmospheric O_2 from ocean nutrient cycles have also been small. Even if changes in nutrient cycles are not negligible, the long-term flux of O_2 across the air-sea interface could be adequately constrained by accurate measurements of dissolved O_2 and nutrient concentrations in the upper ocean.

Another limitation is that the resolution of the residual change in O_2 due to the biosphere would be significantly limited by the uncertainty in fossil-fuel O_2 consumption. The uncertainty in total fossil-fuel O_2 consumption cannot easily be reduced to below $\pm 10\%$ or currently $\pm 0.6 \cdot 10^{14}$ moles/yr (Keeling, 1988, p. 97). This uncertainty will probably increase in the future as consumption of fossil fuels increases. Notwithstanding this limitation, a measurement of the total change in O_2 would pose a tight constraint on the total oxidative source of CO_2 (i.e. the sum of the fossil fuel and biospheric sources) because the average reduction levels of fossil fuels and biomatter differ by less than 40% (Keeling, 1988). Note that a constraint on the total oxidative source of CO_2 is what is most needed for constraining models of ocean uptake of CO_2.

Important applications for atmospheric O_2 measurements would not be limited to seasonal and secular time scales. Background concentrations of atmospheric CO_2 also exhibit interannual variations of the order of 1 ppm which correlate with the Southern Oscillation Index (Bacastow *et al.*, 1980), and spatial gradients in the annual mean concentration (Keeling *et al.*, 1984; Kohmyr *et al.*, 1985). The cause of these variations is not fully understood, and measurements of the corresponding changes in atmospheric O_2 would be valuable as they would constrain the relative contribution of terrestrial and marine processes. Also, measurements which are conducted in proximity to cities, forests, or other ecosystems could be of interest. The ratio of the fluctuations in oxygen and carbon dioxide mole fractions on diurnal or shorter time scales would provide a measure of the reduction level of the organic materials which are exchanging mass with the atmosphere. An example of such a study is the measurements in urban air described below.

In summary, there is scarcely a subject in atmospheric science which is more fundamental yet so poorly understood as the variability of the atmospheric O_2 mole fraction. Measurements of atmospheric O_2 mole fraction would be an important complement to measurements of atmospheric CO_2 and could have a major impact on studies of the global carbon cycle and its perturbation due to human activities. The key requirement, which until recently has been lacking, is the ability to detect variations of the order of 1 ppm in the atmospheric O_2 mole fraction.

3. Experimental Methods

The technique reported here for measuring oxygen mole fraction is based on

resolving small changes in the relative refractivity of H_2O-free air, defined by

$$\tilde{r}(\lambda_1, \lambda_2) = \frac{n(\lambda_1) - 1}{n(\lambda_2) - 1}, \tag{5}$$

where $\lambda_1 = 2537.2687$ Å and $\lambda_2 = 4359.5622$ Å are spectral lines of ^{198}Hg, and where n is the refractive index. The precise choice of wavelengths is not critical because $n - 1$ varies slowly with wavelength.

At low densities the refractive index of a pure gas is given by

$$n - 1 = 2\pi\rho\alpha, \tag{6}$$

where ρ is the number density (molecules per cm^3), and α is the mean (averaged over orientation and quantum states) molecular polarizibility. Also, the refractive index of a gas mixture is given by

$$n - 1 = 2\pi\rho \sum_i X_i \alpha_i = \sum_i X_i (n_i - 1), \tag{7}$$

where the X_i refers to the mole fraction of species i, ρ is the total number density, and n_i is the refractive index of species i at density ρ.

It follows from Equations (5) and (7) that relative refractivity of air varies with abundance of species i according to

$$\delta\tilde{r}(\lambda_1, \lambda_2) = S_i \cdot \delta X_i, \tag{8}$$

where

$$S_i = \frac{n_i(\lambda_2) - 1}{n_{air}(\lambda_2) - 1} \cdot \frac{\tilde{r}_i(\lambda_1, \lambda_2) - \tilde{r}_{air}(\lambda_1, \lambda_2)}{1 - X_i}, \tag{9}$$

where δX_i is the change in mole fraction of species i under the constraint that the relative abundances of all other species (i.e. the ratios X_j/X_k where $j, k \neq i$) remain constant. The derivation of Equation (9) is left to Appendix 1. If changes in $\tilde{r}$ in H_2O-free air are measured, and the measurements are corrected for variations in CO_2 and other gases, then the residual change in $\tilde{r}$ yields, using Equation (8), the change in the O_2 mole fraction of air on a basis which differs negligibly from a basis consisting only of N_2, O_2, and the inert gases. Table I summarizes data for air and its primary constituents for the refractive indicies at 4360 Å, the relative refractivities between 4360 Å and 2537 Å, and the relative refractivity sensitivity coefficients.

Departures from Equation (6) have been observed at elevated densities, i.e. $(n - 1)/\rho$ varies with density (see, e.g., Hill *et al.*, 1969). It follows that the relative refractivity of a gas, in general, also varies with density. This can be expressed in a power expansion about zero density according to

$$\tilde{r}(\lambda_1, \lambda_2) = a(\lambda_1, \lambda_2) + b(\lambda_1, \lambda_2)\,[n(\lambda_2) - 1] + \cdots \tag{10}$$

a and b are virial coefficients of the relative refractivity and where $n(\lambda_2) - 1$ has

been used as the measure of density. Recent measurements on air at 2537 and 4360 Å yielded $b = 0.0157 \pm 0.0006$ (Keeling, 1988, p. 153). The implication of this density dependence on the relative refractivity measurements is discussed further below. The density-dependent corrections to the sensitivity coefficients derived from Equation (9) are insignificant in the present context.

Relative refractivities are measured on a novel interferometer shown in Figure 1. Both arms of the interferometer are formed between just two pieces of optics: a 5.3 cm-thick plane-parallel fused-silica plate which serves as the beam-splitter and recombining surface, and a corner-cube retro-reflector. This arrangement is advantageous because the interferometer is insensitive to vibrations and requires no precise alignments.

A 61.17 cm-long stainless-steel cylinder with four parallel boreholes is located between the plate and the corner cube. All four boreholes are sealed with a single pair of fused-silica windows. The light beam corresponding to one arm of the interferometer travels first down one upper borehole, and returns through the diagonally-opposite lower borehole. The diagonally-opposite boreholes are connected internally to form a single cell. The total path length of each cell is thus 122.34 cm. In order to reduce the sensitivity of the interferometer to temperature and humidity changes in ambient air, the sensitive beams outside of the cells are enclosed within hermetically sealed vessels.

The interferometer is illuminated with a low-pressure electrodeless lamp filled with a trace of isotopically pure ^{198}Hg and 3 torr of Ar. The ^{198}Hg lines of this lamp are known to 0.0001 Å and have been recommended as absolute

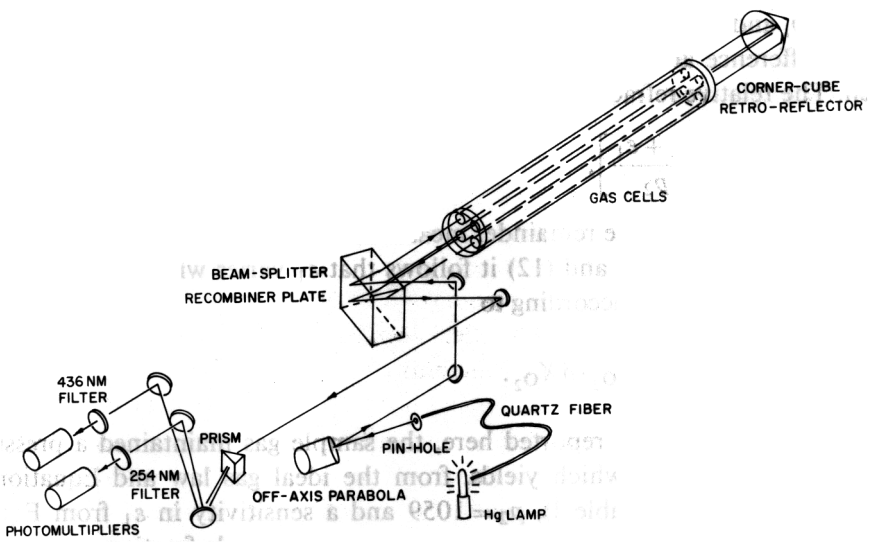

Fig. 1. Interferometer used to measure changes in relative refractivity. The diagonally opposite bore holes are coupled in pairs to form two cells, one along each arm of the interferometer.

length standards (Kaufman, 1962). The ^{198}Hg lamp source was chosen based on its convenience and low cost, although other monochromatic sources (e.g. laser or lamp) alternatively could have been used. In fact, some advantage would have been gained using a source with an ultraviolet line shorter than 2537 Å since this would lead to a higher sensitivity coefficient S_{O_2} .

The output of the lamp is transmitted through a quartz fiber onto a pinhole located at the focus of a parabolic mirror. The emergent collimated beam is stopped down with a circular aperture and is divided into two beams by a beam-splitter coating on the front face of the beam-splitter plate (note that the beam-splitter coating only covers half of the front face of the beam-splitter plate). The two beams then travels complementary paths through the interferometer and are recombined at the beam-splitter plate. The 4360 and 2537 Å components of the recombined beam are resolved by a quartz prism, isolated with narrow-band interference filters, and detected by photomultipliers. The photomultiplier anode currents are converted to voltages through a 350 Hz bandwith electrometer and are read by a system computer after 12-bit analogue-to-digital conversion.

The interferometer is operated with one of the two cells (hereafter refered to as the sample cell) filled with a flowing air sample at an actively stabilized pressure. With the other cell (hereafter refered to as the scanning cell) evacuated, the optical path difference of the interferometer in units of integral orders of interference (or fringes) is given by

$$p_i + \varepsilon_i = \frac{[L]\,[n(\lambda_i) - 1]}{\lambda_i} \tag{11}$$

where p_i and ε_i are the integral and fractional-fringe contributions to the optical path difference at vacuum wavelength λ_i, and L is the total path length of the cell. The relative refractivity is thus given by

$$\bar{r} = \left[\frac{\lambda_1}{\lambda_2}\right]\left[\frac{p_1 + \varepsilon_1}{p_2}\right], \tag{12}$$

where ε_1 is the λ_1-fringe remainder measured relative to the p_2^{th} fringe.

From Equations (8) and (12) it follows that ε_1 varies with the O_2 mole fraction of the air sample according to

$$\delta\varepsilon_1 = \left(\frac{\lambda_2}{\lambda_1}\right) p_2 \cdot S_{O_2} \cdot \delta X_{O_2}$$

For the measurements reported here, the sample gas maintained a pressure of 1935 torr (at 22 °C) which yields, from the ideal gas law and Equation (11) (see data for air in Table I), $p_2 = 1059$ and a sensitivity in ε_1 from Equation (13) of 1.11×10^{-4} of a fringe per ppm change in O_2 mole fraction.

The fringe remainder ε_1 is measured by bleeding dry compressed air into the scanning cell from vacuum to 20 torr and recording the temporal inter-

Table I. Refractivity data for air and its primary constituents

Species	Mole fraction in dry air X_i	Relative refractivity $\tilde{r}$(4360 Å, 2537 Å)	Refractivity at 0 °C, 760 torr n(4360 Å)−1	Sensitivity factor, S_i (ppm^{-1})	Relative sensitivity S_i/S_{O_2}
Air	–	1.06902[a]	2.965×10^{-4} [a]		
N_2	78.067%	1.06203[b]	3.023×10^{-4} [c]	–	
O_2	20.946%[d]	1.0971[e]	2.754×10^{-4} [e]	3.30×10^{-8}	1.00
H_2O	0 to 3%[f]	1.1065[b]	2.517×10^{-4} [g]	3.18×10^{-8}	0.96
Ar	0.934%[h]	1.06126[b]	2.854×10^{-4} [i]	-0.75×10^{-8}	−0.24
CO_2	339 ppm[j]	1.07301[b]	4.562×10^{-4} [k]	0.614×10^{-8}	0.186
Ne	181.8 ppm[h]	1.0244[l]	6.754×10^{-5} [l]	-1.02×10^{-8}	−0.31
He	5.24 ppm[h]	1.0250[l]	3.511×10^{-5} [m]	-0.52×10^{-8}	−0.16
Kr	1.14 ppm[h]	1.0855[n]	4.357×10^{-4} [n]	2.42×10^{-8}	0.73
CH_4	1.7 ppm[o]	1.09350[b]	4.513×10^{-4} [p]	3.73×10^{-8}	1.13
H_2	0.5 ppm[h]	1.0912[g]	1.417×10^{-4} [p]	1.06×10^{-8}	0.32
N_2O	0.30 ppm[q]	1.09921[b]	5.138×10^{-4} [g]	5.23×10^{-8}	1.59
CO	0.02–0.25 ppm[r]	1.10533[b]	3.418×10^{-4} [s]	4.18×10^{-8}	1.27
O_3	0.0–0.1 ppm	–	–	4.9×10^{-7} [b]	15.8

[a] Formula (32) in Owens (1967).
[b] Keeling (1988).
[c] Formula (3) in Peck and Khana (1966).
[d] Machta and Hughes (1970).
[e] Formula (6) in Ladenburg and Wolfsohn (1932).
[f] Typical range in most air.
[g] Formula (5) in Zeiss and Meath (1977).
[h] NOAA (1976).
[i] Formula in Peck and Fischer (1964).
[j] Keeling *et al.* (1982).
[k] Formula in Old *et al.* (1971).
[l] Formula in Cuthbertson and Cuthbertson (1932).
[m] Formula in Mansfield and Peck (1969).
[n] Formula in Koch (1949).
[o] Khalil and Rasmussen (1986).
[p] Formula (2.18) in Kerl (1982).
[q] Weiss (1981).
[r] Logan *et al.* (1981).
[s] Formula in Cuthbertson and Cuthbertson (1920).

ference fringes on a micro-computer. An algorithm of Snyder (1980) is used to resolve the relative phasing of the λ_1 and λ_2 signals. One of the λ_2 fringes near the center of the scan is selected as the reference fringe and ε_1 is determined by the phase of the λ_1 fringes relative to the reference fringe. Once the pressure-scan and fringe-processing cycle is complete, and the reference cell is reevacuated to less than 0.5 torr, the cycle is repeated. The entire cycle requires approximately 25 seconds and yields ε_1 with an imprecision for replicate scans of 2×10^{-4} of fringe corresponding to a sensitivity in the oxygen mole fraction of 2 ppm.

The sensitivity of ε_1 to changes in sample density is given by

$$\delta\varepsilon_1 = \left[\left(\frac{dp_1}{dp_2}\right)_{\text{samp}} - \left(\frac{dp_1}{dp_2}\right)_{\text{scan}}\right](\delta p_2)_{\text{samp}},$$

where $(dp_1/dp_2)_{\text{samp}}$ and $(dp_1/dp_2)_{\text{scan}}$ are the frequency ratios of the λ_1 and λ_2 fringes produced by changes in sample-gas density and scanning-gas density respectively, and $(\delta p_2)_{\text{samp}}$ is the change in sample-gas density expressed in units of λ_2 fringes. In general, the difference between the two frequency ratios is non-zero for two reasons: (1) the composition of the sample gas can be different from the composition of the scanning gas, and (2) the relative refractivity of the sample gas is shifted relative to the relative refractivity of the scanning gas according to Equation (10). For these measurements only the second contribution is significant. The second contribution to the frequency-ratio difference is given by

$$\left(\frac{dp_1}{dp_2}\right)_{\text{samp}} - \left(\frac{dp_1}{dp_2}\right)_{\text{scan}} = 2\left[\frac{\lambda_2}{\lambda_1}\right] b(\lambda_1, \lambda_2)\cdot[n_{\text{samp}}(\lambda_2) - 1].$$

Equation (15) is derived in Appendix 2. For the measurements reported here the frequency-ratio difference derived from Equation (15) amounts to 3.8×10^{-5}. This implies that ε_1 would have varied by 3.8×10^{-5} of a fringe for every λ_2 fringe which elapsed due to changes in sample-gas density.

The errors induced by density changes in the sample gas are reduced by actively stabilizing the pressure in a buffer volume upstream of the sample cell. This is achieved using a capacitance differential-pressure gauge to generate an error signal proportional to the pressure difference between the buffer and reference volumes. The error signal is fed back through a control circuit (MKS Instruments 250B controller) which makes settings on an automatic regulating valve at the inlet to the buffer volume. Long-term drift in the sample-gas density, caused e.g. by changes in reference-volume temperature, is corrected for by making occasional manual adjustments on the set-point of the flow controller. For the measurements reported here, the sample-cell density was stabilized to the level of ± 0.5 of a λ_2 fringe which leads to maximum density-induced changes in ε_1 of $\pm 2 \times 10^{-5}$, or maximum errors of 0.2 ppm in the O_2 mole fraction.

The instrument was tested on ambient air from outside the Engineering Sciences Laboratory at Harvard University in Cambridge, Massachusetts. Air was drawn from outside a first floor window located about 10 m from Oxford Street, a moderately busy street. The air was drawn through an inlet system into a manifold and from the manifold into the oxygen analyzer. The inlet system consisted successively of a 12 m inlet line, a cold trap at −78 °C, a membrane filter for removing particulates, a diaphram compressor pump, and a second cold trap at −78 °C. Previous tests (involving saturating, drying, and then analyzing for differences in O_2 mole fraction) showed that this procedure

did not alter the O_2 mole fraction at the sensitivity of the instrument. The manifold allowed alternately ambient air or reference gas to be introduced into the interferometer. When a reference gas was used, the ambient air stream was vented to the room through a back pressure regulator in order to maintain a constant flow rate and steady pressures in the inlet system at all times. This was necessary because pressure fluctuations were found to lead to fluctuations in O_2 mole fraction (presumably due to differential physisorption of O_2 and N_2).

Between the manifold and the interferometer the flow passed successively through a cold trap at −78 °C, a sub-micron filter, an automatic flow control valve, a ballast volume, and a fine metering valve. The materials exposed to the gas included stainless steel, glass, and teflon, and trace amounts of viton and Apiezon N vacuum grease. The sample attained a pressure of 1935 torr in the sample cell at a flow rate of 680 cm^3 STP/min. With the volume spanned by the inlet manifold and sample cell of 380 cm^3, this yielded a flushing time constant of approximately 1.3 minutes.

Carbon dioxide concentrations were measured in the exhaust line of the interferometer with a non-dispersive dual-cell infrared analyzer (Binos) operated at ambient pressure. The reference cell of infrared analyzer was continually flushed with an air stream with nominally 340 ppm CO_2 at ambient pressure. Carbon dioxide concentrations are reported on a scale which is linear in instrument response and based on a two-point calibration with reference gases at 340.0 ± 0.5 ppm and 380.0 ± 0.5 ppm. The imprecision of replicate readings on the adjusted scale was ± 0.1 ppm.

The interferometer responds not only to changes in sample gas composition, but also responds to changes in ambient room temperature. Because of its large thermal mass, the interferometer responds to temperature on a time scale of several hours. To correct for thermal drift, the interferometer sample cell was flushed with a reference gas at intervals of about two hours. This reference gas cylinder was filled with air compressed at the Scripps Pier in La Jolla, California while the wind was blowing off the ocean. It was determined to have a concentration of 343.9 ppm carbon dioxide. The interferometer response from three or four consecutive calibrations was least-squares fitted to a second or third order polynomial. This established a calibration baseline which was subtracted from the interferometer readings with ambient air on a point-for-point basis. Tests using different order polynomials and different consecutive sets of readings indicated that the baseline could be interpolated with a precision of approximately ± 2.0 ppm O_2.

4. Results and Discussion

Ambient air was monitored on the evening of 25 October 1986 and throughout the next day. Figure 2 shows the output of the CO_2 and O_2 analyzers over a selected time interval on 26 October which spans three calibration intervals.

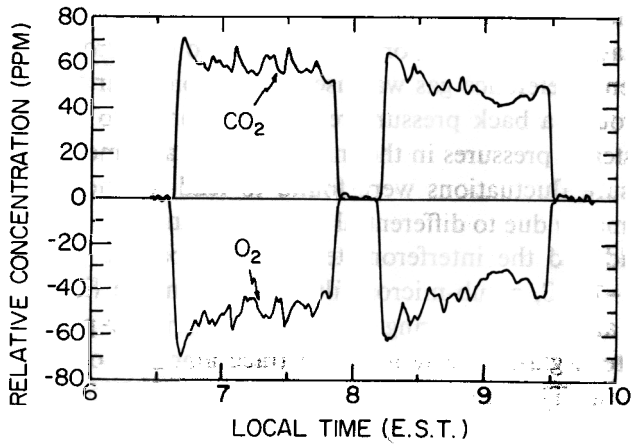

Fig. 2. Time trends of the response of the O_2 and CO_2 analyzers expressed as the difference between ambient air and the reference gas in ppm (mole fraction). Oxygen data has not been corrected for CO_2 interference and possible interference of other gases.

Figure 3 shows a fraction of this interval in closer detail. The output of both analyzers is expressed in terms of the difference between ambient air and the reference gas in units of ppm in the mole fraction. The individual readings of the oxygen and carbon dioxide analyzer, taken at around 30 second intervals, have been smoothed with a four point running mean. The output of the oxygen analyzer has been scaled according to the sensitivity factor in Equation (8) but has not been corrected for the interference of carbon dioxide and other gases.

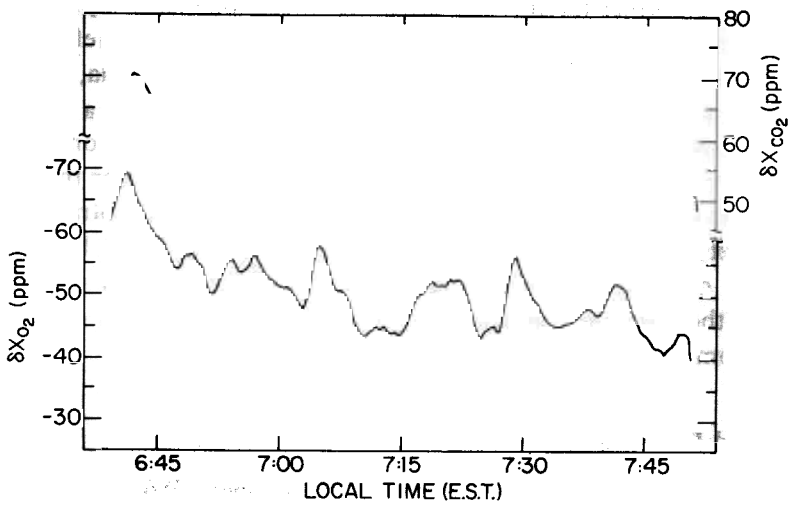

Fig. 3. Same data as Figure 2. O_2 axis has been inverted to allow for better visualization of correlations.

The CO_2 corrections are the wrong sign and too small, by a factor of four, to account for the observed response. Other gases, most notably CO and hydrocarbons, which can be present in the 0 to 10 pm level in urban air, might also account for a fraction of the response of the O_2 analyzer. However, because these gases increase the relative refractivity of air and would tend to increase in abundance with increasing CO_2, their contribution to the change in relative refractivity is, again, of the wrong sign. The observed decrease in the relative refractivity with increasing CO_2 must be caused by changes in O_2 mole fraction.

The data show fluctuations in CO_2 and O_2 mole fraction that are strongly anti-correlated on time scales ranging from minutes to hours. The level of instrumental noise on the oxygen analyzer is evident from the scale of fluctuations during the calibration intervals.

A summary of the broad time trend in CO_2 and O_2 mole fractions is shown in Figure 4. These data represent the average concentration recorded between calibration intervals on both 25 and 26 October. These O_2 data have been corrected for the instrumental CO_2 interference according to Equation (8) based on the difference between ambient CO_2 and the 343.9 ppm reference gas. On the evening of 26 October, the atmosphere was relatively still, and ambient CO_2 increased from 350 to 410 ppm overnight while O_2 decreased by a similar amount. A storm system moved in on 26 October accompanied by increasing winds, a decrease in CO_2 to near background levels, and a comparable increase in O_2.

In order to explore further the extent of the correlation between O_2 and CO_2 mole fractions, time intervals of approximately five minutes duration were selected during which stable readings were recorded on both analyzers. The CO_2

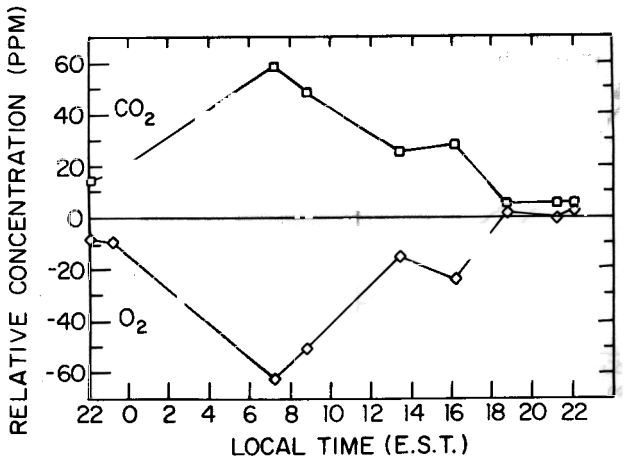

Fig. 4. Diurnal trend in oxygen and carbon dioxide. The data represent the average ambient levels of oxygen and carbon dioxide recorded between calibration intervals. The data are expressed in units of ppm (mole fraction) difference between ambient air and reference gas. The O_2 data have been corrected for CO_2 interference but not for possible interferences of other gases.

Table II. Measured difference between ambient oxygen and carbon dioxide mole fractions and reference gas in ppm

Date	Time	CO_2	O_2	Date	Time	CO_2	O_2
25 Oct. 86	22:44	12.5	−5.6	26 Oct. 86	14:21	28.8	−19.6
	23:31	17.0	−8.4		15:14	33.1	−29.9
	23:17	13.5	−6.3		16:16	24.3	−16.9
26 Oct. 86	0:16	18.3	−9.6		16:52	17.0	−7.9
	6:50	60.0	−62.9		18:14	4.4	1.2
	7:13	55.8	−51.8		18:35	7.0	−1.3
	7:21	62.2	−60.6		19:07	3.9	6.8
	7:36	56.2	−53.2		20:26	9.3	−1.0
	8:46	49.3	−48.6		20:43	14.1	−7.2
	9:09	42.1	−37.0		21:02	2.8	6.5
	10:58	27.6	−18.6		22:09	4.9	5.0
	11:16	21.4	−12.2		22:23	4.9	7.3
	13:33	26.2	−14.8				

and O_2 readings were averaged over each interval and the O_2 readings corrected for CO_2 interference. These data are summarized in Table II and the CO_2-corrected O_2 readings are plotted against CO_2 readings in Figure 5. The data yield a linear correlation coefficient ($r = 0.991$) which is valid at better than the 99.9% confidence level, and a linear regression slope of -1.145 ± 0.023 (1σ) ppm O_2 per ppm CO_2. Based on the imprecision for replicate scans of ± 2 ppm, the imprecision for a five minute average is estimated to be ± 0.6 ppm. The ambiguity of the calibration baseline leads to an additional imprecision of

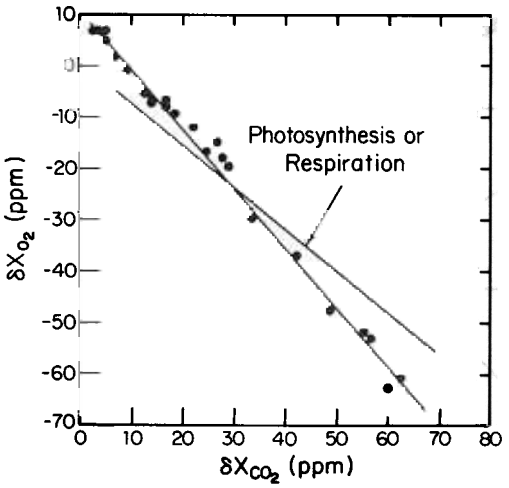

Fig. 5. Correlation of ambient O_2 versus CO_2 concentrations measured on 25 and 26 October, 1986. Concentrations reported as mole fraction difference between ambient air and reference gas in ppm. The O_2 data have been corrected CO_2 interference but not for possible interferences of other gases. The line through the data represents a linear least-squares fit to the data. The line labeled photosynthesis or respiration corresponds to the slope which would obtain for the combustion of carbohydrate.

approximately ±2 ppm, as discussed above. The standard deviation of the residuals to the fit is ±2.4 ppm which is an independent upper estimate to the imprecision of the measurements because some of the variance in the fit could be due to atmospheric variability.

The accuracy of the O_2 measurements is additionally limited by the interferences of CO, hydrocarbons, and ozone which were not measured simultaneously. CO emissions from automobiles in an urban environment average approximately 17% of total C emission (Holey, 1987), so that CO concentrations as high as 15 ppm or an interference of 20 ppm O_2 may have occured during times of elevated CO_2. Although non-methane hydrocarbons (NMHC) concentrations have been observed to be as high as 5 ppm in Boston in the summer, a typical summer value is around 400 ppb (Secton and Westberg, 1984), and lower NMHC concentrations would be expected under the cool (~10 °C) conditions under which these measurements were carried out. Because the relevant refractivity data for typical atmospheric hydrocarbons is not available, it is difficult, at present, to assess the impact of NMHCs on the O_2 measurements. Ground-level O_3 concentrations in late October in Cambridge rarely exceed 50 ppb (based on measurements conducted at Harvard for educational purposes) which would correspond to a maximum interference in the O_2 measurements of 0.8 ppm.

The slope of the correlation plot contains information about the average reduction level of the materials oxidized in the local environment at the time of the measurements. A detailed interpretation of the correlation would require an assessment of all interfering species. In spite of this limitation, an analysis of the observations is presented which accounts only for interferences of CO_2 and CO. This analysis serves to illustrate the method of applying O_2/CO_2 studies for estimating reduction levels, and serves to test whether the reported measurements are broadly consistent with the expectations for urban air.

Allowing for formation of CO, we can represent the combustion of fuel according to

$$CH_x + \left(-\frac{y}{2} + \frac{x}{4} \right) O_2 \rightarrow (1-y)\cdot CO_2 + y\cdot CO + \frac{x}{2}\cdot H_2O, \tag{16}$$

where CH_2 represents the composition of the fuel and y represents the fraction of C emitted as CO. The reduction level of the fuel is given by

$$(RL) = 1 + \frac{x}{4} \tag{17}$$

If changes in the atmospheric abundances of O_2, CO_2, and CO are determined only by Equation (16), then the atmospheric mole fractions of these species are related according to

$$\delta X_{O_2} = -(1 - X_{O_2}) \left[\frac{1 - \frac{y}{2} + \frac{x}{4}}{-y} \right] \cdot \delta X_{CO_2}, \tag{18}$$

$$\delta X_{CO} = \left[\frac{y}{1-y}\right] \cdot \delta X_{CO_2}$$

We now define the quantity r to be the ratio of the change in the relative refractivity of air scaled, according to Equation (9), in units of ppm O_2 to the change in X_{CO_2}. It follows that

$$r \cdot \delta X_{CO_2} = \delta X_{O_2} + \frac{S_{CO_2}}{S_{O_2}} \cdot \delta X_{CO_2} + \frac{S_{CO}}{S_{O_2}} \cdot \delta X_{CO} \cdot \tag{20}$$

From Equation (17) to (20) it follows that

$$(RL) = \frac{1-y}{1-X_{O_2}} \left[-r + \frac{S_{CO_2}}{S_{O_2}} + \frac{y}{1-y} \cdot \frac{S_{CO}}{S_{O_2}}\right] + \frac{y}{2} \tag{21}$$

Equation (21) has been used to calculate the observed reduction level listed in Table III where r has been identified with the slope of the least-squares fit between the scaled interferometer response and the measured CO_2 concentrations (i.e. $r - S_{CO_2}/S_{O_2} = -1.145$). The calculation allows for experimental uncertainties and for a range of CO emission factors from a low of 0% to high of 17% corresponding to the emission factors for automobiles in an urban environment (Holey, 1987). The reported uncertainty in the reduction level is a mini-

Table III. Comparison of reduction level of common fuels with the reduction level implied by the O_2/CO_2 correlations

Observed reduction level[a]	1.50 ± 0.06
Gasoline[b]	$1.52 - 1.56$
Natural gas[c]	$1.83 - 2.00$
Fuel oil[d]	$1.39 - 1.44$

[a] Computed according to Equation (21). The calculation assumes that $8.5 \pm 8.5\%$ of the C is emitted as CO and the reported error limits (1 sigma) allow for the variance to the least squares fit between the scaled instrument response and measured CO_2 concentrations, the inaccuracy of scaling of carbon dioxide analyzer response, and the above uncertainty in the CO emission factor, assuming errors are statistically independent.

[b] Based on range of composition spanned by the two types of gasoline listed in Mark's Handbook (1967).

[c] Based on range of composition spanned by fuels, Index 1 and Index 7 from Cardwell and Benton (1971).

[d] Based on range of composition spanned by the three types of fuel oil listed in Mark's Handbook (1967).

mum uncertainty because interferences of hydrocarbons and O_3 have not been assessed. The observed reduction level of 1.50 ± 0.06 falls within the range for liquid fuels. The observations are therefore consistent with the notion that automobiles should be the dominant local CO_2 source and O_2 sink.

5. Conclusions

Short-term fluctuations in atmospheric oxygen mole fraction have been detected in the air in Cambridge, Massachusetts by interferometric detection of changes in relative refractivity. The fluctuations in oxygen are strongly anti-correlated with changes in carbon dioxide, and the ratio in amplitude of the changes in oxygen and carbon dioxide mole fractions is consistent with the ratio expected from gasoline burning. The precision of the oxygen measurements is ± 2 ppm in the mole fraction. It is likely that modest improvements in the instrument would yield a resolution of 0.5 ppm or better.

These measurements are significant because they demonstrate the feasibility of detecting variations in oxygen mole fraction at the level expected in background air. Measurements of O_2 mole fraction in background air would be of broad biogeochemical interest. Several of the issues which could be addressed with such measurements include: (1) assessing the magnitude of seasonal exchange of O_2 across the air-sea interface which is relevant for understanding biological productivities of ocean surface waters, and (2) assessing the net rate of oxidation of biomatter which is relevant for understanding the recent rise in CO_2.

A limitation of the interferometric oxygen detection is the need to assess interferences from CO_2, CO, hydrocarbons, O_3, and possibly other species. While the lack of data for such species significantly limits the accuracy of the present measurements, the magnitude of these interferences, aside from CO_2, would generally be much lower in background air. Variations in CO, hydrocarbons, and O_3 in background air would generally lead to O_2 interferences smaller than 1 ppm O_2. With routine measurements it would be possible to assess the magnitude of these interferences to a combined error of a few tenths of a ppm.

A more serious limitation for long-term O_2 measurements is the need for highly stable reference gases. The issue is most serious for accurate determination of the long-term decline in the O_2 mole fraction, where a stability of better than 0.3 ppm per year would be desirable. For assessing the magnitude of seasonal and other short-term variations, the stability of high pressure cylinders of compressed air is probably adequate, although this remains to be demonstrated.

Appendix 1

Equation (9) is most simply derived for the case of a binary mixture. We let X_a and X_b denote the mole fractions of constituent a and b such that

$$X_a + X_b = 1. \tag{22}$$

We then define the refractivity $r_{\text{mix}} = n_{\text{mix}} -$ of the mixture. Equation (7) then becomes

$$r_{\text{mix}} = r_a X_a + r_b X_b, \tag{23}$$

where r_a and r_b denote the refractivities of constituents a and b. The relative refractivity is then given by

$$\tilde{r} = \frac{r_{\text{mix}}(\lambda_1)}{r_{\text{mix}}(\lambda_2)}. \tag{24}$$

Substituting Equation (23) into Equation (24) and eliminating X_b via Equation (22) yields

$$\tilde{r} = \frac{[r_a(\lambda_1) - r_b(\lambda_1)]X_a + r_b(\lambda_1)}{[r_a(\lambda_2) - r_b(\lambda_2)]X_a + r_b(\lambda_2)}. \tag{25}$$

Differentiating with respect to X_a

$$\frac{1}{\tilde{r}}\frac{d\tilde{r}}{dX_a} = \frac{r_a(\lambda_1) - r_b(\lambda_2)}{r_{\text{mix}}(\lambda_1)} - \frac{r_a(\lambda_2) - r_b(\lambda_2)}{r_{\text{mix}}(\lambda_2)} \tag{26}$$

and eliminating r_b using Equations (23) and (22) yields

$$\frac{1}{\tilde{r}}\frac{d\tilde{r}}{dX_a} = \frac{1}{1 - X_a}\left[\frac{r_a(\lambda_1) - r_{\text{mix}}(\lambda_1)}{r_{\text{mix}}(\lambda_1)} - \frac{r_a(\lambda_2) - r_{\text{mix}}(\lambda_2)}{r_{\text{mix}}(\lambda_2)}\right] \tag{27}$$

or

$$\frac{1}{\tilde{r}}\frac{d\tilde{r}}{dX_a} = \frac{1}{1 - X_a}\left[\frac{r_a(\lambda_1)}{r_{\text{mix}}(\lambda_1)} - \frac{r_a(\lambda_2)}{r_{\text{mix}}(\lambda_2)}\right] \tag{28}$$

Substituting from Equation (24) into Equation (28) we have

$$\frac{d\tilde{r}}{dX_a} = \frac{1}{1 - X_a}\frac{r_{\text{mix}}(\lambda_1)}{r_{\text{mix}}(\lambda_2)}\left[\frac{r_a(\lambda_1)}{r_{\text{mix}}(\lambda_1)} - \frac{r_a(\lambda_2)}{r_{\text{mix}}(\lambda_2)}\right]. \tag{29}$$

or

$$\frac{d\tilde{r}}{dX_a} = \frac{1}{1 - X_a}\frac{r_a(\lambda_2)}{r_{\text{mix}}(\lambda_2)}\left[\frac{r_a(\lambda_1)}{r_a(\lambda_2)} - \frac{r_{\text{mix}}(\lambda_1)}{r_{\text{mix}}(\lambda_2)}\right] \tag{30}$$

or

$$\frac{d\tilde{r}}{dX_a} = \frac{n_a(\lambda_2)}{n_{\text{mix}}(\lambda_2) - 1}\frac{1}{1 - X_a}(\tilde{r}_a - \tilde{r}), \tag{31}$$

where $\tilde{r}_a = r_a(\lambda_1)/r_a(\lambda_2)$ is the relative refractivity of constituent a.

Equation (31) can also be applied directly to a mixture containing more than two components and thus Equations (8) and (9) follow directly. In this case, component b is identified with the sum of all species other than a. The use of Equation (31) to describe relative-refractivity changes in a multicomponent mixture requires that the transformation which alters the mole fraction of species a does not alter the relative proportions of the other constituents.

Appendix 2

This appendix provides a derivation of Equation (15). According to Equation (11) the frequency ratio of the fringes produced by changes in sample gas density is

$$\left(\frac{dp_1}{dp_2}\right)_{\text{samp}} = \frac{\lambda_2}{\lambda_1}\frac{dn(\lambda_1)}{dn(\lambda_2)}. \tag{32}$$

Also, from Equation (10) we have

$$n(\lambda_1) - 1 = a(\lambda_1, \lambda_2)\,[n(\lambda_2) - 1] + b(\lambda_1, \lambda_2)\,[n(\lambda_2) - 1]^2 + \cdots \tag{33}$$

From Equations (33) and (32), we have

$$\left(\frac{dp_1}{dp_2}\right)_{\text{samp}} = \left(\frac{\lambda_2}{\lambda_1}\right) a(\lambda_1, \lambda_2) + 2b(\lambda_1, \lambda_2)\left(\frac{\lambda_2}{\lambda_1}\right)(n(\lambda_2) - 1) + \cdots$$

Now, because the scanning gas is effectively at zero density, and because its composition differs negligibly from sample gas, we have

$$\left(\frac{dp_1}{dp_2}\right)_{\text{scan}} = \left(\frac{\lambda_2}{\lambda_1}\right) a(\lambda_1, \lambda_2)$$

Subtracting Equation (35) from Equation (34) and neglecting higher-order terms yields Equation (15).

Acknowledgements

I am indebted to Dr Jim Anderson whose unfailing support, enthusiasm, and optimism has played an essential role in the development of the interferometric oxygen analyzer. Nate Hazen assisted in substantial aspects of the mechanical design of the interferometer.

I am grateful to Dr Steve Wofsy for lending the CO_2 analyzer and CO_2 calibration gases and to Bill DeRoo for his assistance in assembling electronic hardware and developing software.

This material is based upon work supported by the National Science Foundation under Grant AEO-84-12224.

References

Bacastow, R. B., Adams, J. A., Keeling, C. D., Moss, D. J., Whorf, T. P., and Wong, C. S., 1980, Atmospheric carbon dioxide, the southern oscillation, and the weak 1975 El Nino, *Science* **210**, 66–68.

Benedict, F. G., 1912, *The Composition of the Atmosphere with Special Reference to its Oxygen Content*, Carnegie Institution of Washington, Washington, D.C.

Broecker, W. S., Takahashi, T., Simpson, H. J., Peng, T.-H., 1979, Fate of fossil fuel carbon dioxide and the global carbon budget, *Science* **206** (4417), 409–418.

Broecker, W. S. and Peng, T.-H., 1982, *Tracers in the Sea*, Lamont-Doherty Geological Observatory, Palisades, New York.

Carpenter, T. M., 1937, The constancy of the atmosphere with respect to carbon dioxide and oxygen content, *J. Amer. Chem. Soc.* **59**, 358–360.

Cardwell, L. E., Benton, L. F., 1971, U.S. Bureau of Mines Information Circular 8518, Analysis of Natural Gases.

Cuthbertson, C. and Cuthbertson, M., 1920, On the refraction and dispersion of carbon dioxide, carbon monoxide, and methane, *Proc. Royal Soc. London, Series A* **97**, 152–159.

Cuthbertson, C. and Cuthbertson, M., 1932, The refraction and dispersion of neon and helium, *Proc. Royal Soc. London, Series A* **135**, 40–47.

Enting, I. G. and Pearman, G. I., 1987, Description of a one-dimensional carbon cycle model calibrated using techniques of constrained inversion, *Tellus* **39B**, 459–476.

Eppley, R. W. and Peterson, B. J., 1979, Particulate organic matter flux and planktonic new production in the deep ocean, *Nature* **282**, 677–680.

Fung, I., Prentice, K., Matthews, E., Lerner, J., and Russel, G., 1983, Three-dimensional tracer model study of atmospheric CO_2: response to seasonal exchanges with the terrestrial biosphere, *J. Geophys. Res.* **88** (C2), 1281–1294.

Giese, A. C., 1973, *Cell Physiology, 4th edn.*, W. B. Saunders, Philadelphia.

Glueckauf, E., 1951, The composition of atmospheric air, in T. Malone (ed.) *Compendium of Meteorology*, American Meteorological Society, Boston, pp. 3–10.

Heimann, M., Keeling, C. D., and Fung, I. Y., 1986, Simulating the atmospheric carbon dioxide distribution with a three dimensional tracer model, in J. R. Trabalka and D. E. Reichle (eds.), *The Changing Carbon Cycle: A Global Analysis*, Springer Verlag, New York, pp. 16–49.

Hill, N. E., Vaughan, W. E., Price, A. H., and Davies, M., 1969, *Dielectric Properties and Molecular Behaviour*, Van Nostrand Reinhold, London.

Holey, T., Environmental Protection Agency, Air Management Division, Personal communication.

Houghton, R. A., Boone, R. D., Fruci, J. R., Hobbie, J. E., Melillo, J. M., Palm, C. A., Peterson, B. J., Shaver, G. R., Woodwell, G. M., Moore, B., Skole, D. L., Myers, N., 1987, The flux of carbon from terrestrial ecosystems to the atmosphere in 1980 due to changes in land use: geographic distribution of the global flux, *Tellus* **39B**, 122–139.

Hughes, E. E., 1968, A simple technique for the absolute determination of atmospheric oxygen, *Environ. Sci. Technol.* **2**(3), 201–203.

Jenkins, W. J. and Goldman, J. C., 1985, Seasonal oxygen cycling and primary production in the Sargasso Sea, *J. Marine Res.* **43**, 465–491.

Kaufman, V., 1962, Wavelengths, energy levels, and pressure shifts in mercury 198, *J. Opt. Soc. Amer.* **52**(8), 866–870.

Keeling, C. D., Bacastow, R. B., and Whorf, T. P., 1982, Measurements of the concentration of carbon dioxide at Mauna Loa Observatory, Hawaii, in W. C. Clark (ed.), *Carbon Dioxide Review: 1982*, Oxford University Press, New York, pp. 377–385.

Keeling, C. D., Carter, A. F., and Mook, W. G., 1984, Seasonal, latitudinal and secular variations in the abundance and isotopic ratios of atmospheric CO_2. 2. Results from oceanic cruises in the tropical Pacific Ocean, *J. Geophys. Res.* **89**(D3), 4615–4628.

Keeling, R. F., 1988, Development of an interferometric oxygen analyzer for precise measurement of the atmospheric O_2 mole fraction, PhD Thesis, Harvard Univ.

Kerl, K., 1982, Determination of mean molecular polarizabilities and second virial coefficients of gases by scanning-wavelength interferometry, *Zeit Physik. Chem. Neue Folge* **129**, 129–148.

Khalil, M. A. K., and Rasmussen, R. A., 1986, Interannual variability of atmospheric methane: possible effects of the El Niño-Southern Oscillation, *Science* **232**, 56–57.

Koch, J., 1949, On the refraction and dispersion of the noble gases krypton and xenon, *Kungl. Fysiografiska Sällskapets i Lund Förhandlingar* **19**(13), 173–187.

Komhyr, W. D., Gammon, R. H., Harris, T. B., Waterman, L. S., Conway, T. J., Taylor, W. R., Thoning, K. W., 1985, Global Atmospheric CO_2 distribution and variations from 1968–1982 NOAA/GMCC CO_2 flask sample data, *J. Geophys. Res.* **90**(D3), 5567–5596.

Krogh, A., 1919, The composition of the atmosphere, *Det Kgl. Danske Videnskabernes Selskab.* **1**, No. 12.

Ladenburg, R. and Wolfsohn, G., 1932, Untersuchungen über die Dispersion von Gasen und Dämpfen and ihre Darstellung durch die Dispersiontheorie. III. Die Dispersion des Sauerstoffs zwischen 6000 und 1920 Å, *Zeit. Physik* **79**, 42–60.

Lockhart, E. E. and Court, A., 1942, Oxygen deficiency in Antarctic air, *Monthly Weath. Rev.* **70**(5), 93–96.

Logan, J. A., 1985, Tropospheric ozone: seasonal behavior, trends, and anthropogenic influence, *J. Geophys. Res.* **90**(D6), 10463–10482.

Machta, L. and Hughes, E., 1970, Atmospheric Oxygen in 1967 to 1970, *Science* **168**, 1582–1584.

Machta, L. E., 1980, Oxygen depletion, in Jacoby (ed.), *Carbon Dioxide Effects Research and Assessment Program: Proceedings of the International Meeting on Stable Isotopes in Tree-Ring Research*, U.S. Dept. of Energy, pp. 125–127.

Mansfield, C. R. and Peck, E. R., 1969, Dispersion of helium, *J. Opt. Soc. Amer.* **59**(2), 199–204.

Marks, L. E. (ed.), 1967, *Mechanical Engineers' Handbook*, 7th edn. McGraw-Hill, New York.

Marland, G. and Rotty, R. M., 1984, Carbon dioxide emissions from fossil fuels: a procedure for estimation and results for 1950–1982, *Tellus* **36 B**, 232–261.

Mook, W. G., Koopmans, M., Carter, A. F., and Keeling, C. D., 1983, Seasonal, latitudinal, and secular variations in the abundance and isotopic ratios of atmospheric carbon dioxide 1. Results from land stations, *J. Geophys. Res.* **88**(C15), 10915–10933.

Neftel, A., Moor, E., Oeschger, H., Stauffer, B., 1985, Evidence from polar ice cores for the increase in atmospheric CO_2 in the past two centuries, *Nature* **315**, 45–47.

NOAA, 1976, *U.S. Standard Atmosphere, 1976*, National Oceanic and Atmospheric Administration, National Aeronautics and Space Administration, United States Air Force, Washington, D.C.

Old, J. G., Gentili, K. L., and Peck, E. R., 1971, Dispersion of carbon dixide, *J. Opt. Soc. Amer.* **61**(1), 89–90.

Owens, J. C., 1967, Optical refractive index of air: dependence on pressure, temperature and composition, *Appl. Opt.* **6**(1), 51–59.

Pearman, G. I. and Hyson, P., 1980, Activities of the global biosphere as reflected in atmospheric CO_2 records, *J. Geophys. Res.* **85**(C8), 4468–4474.

Peck, E. R. and Fisher, D. J., 1964, Dispersion of argon, *J. Opt. Soc. Amer.* **54**(11), 1362–1364.

Peck, E. R. and Khanna, N., 1966, Dispersion of nitrogen, *J. Opt. Soc. Amer.* **56**(8), 1059–1063.

Peng, T.-H. and Broecker, W. S., 1984, Ocean life cycles and the atmospheric CO_2 content, *J. Geophys. Res.* **89**(C5), 8170–8180.

Peng, T.-H., Takahashi, T., Broecker, W. S., and Olafsson, J., 1987, Seasonal variability or carbon dioxide, nutrients, and oxygen in the northern North Atlantic surface water: observations and a model, *Tellus* **39B**, 439–458.

Platt, T., 1984, Primary productivity of the central North Pacific: comparison of oxygen and carbon fluxes, *Deep Sea Res.* **31**(11), 1311–1319.

Sexton, K. and Westberg, H., 1984, Nonmethane hydrocarbon composition of urban and rural atmospheres, *Atmos. Environ.* **18**(6), 1125–1132.

Shepherd, M., 1935, The composition of the atmosphere at approximately 21.5 kilometers, *U.S. Army Stratosphere Flight of 1935 in Balloon Explorer II*, National Geographic Soc., Washington D.C., pp. 117–133.

Shulenberger, E. and Reid, J. L., 1981, The Pacific shallow oxygen maximum, deep chlorophyll maximum, and primary productivity, reconsidered, *Deep Sea Res.* **28A**(9), 901–919.

Siegenthaler, U. and Oeschger, H., 1987, Biospheric CO_2 emissions during the past 200 years reconstructed by deconvolution of ice core data, *Tellus* **39B**, 140–154.

Snyder, J. J., Algorithm for fast digital analysis of interference fringes, *Appl. Opt.* **19**(8), 1223–1225.
Söderlund, R. and Svennson, B. H., 1976, The global nitrogen cycle, in B. Svensson, and R. Söderlund (eds.), *Nitrogen, Phosphorus and Sulphur – Global Cycles, SCOPE Report No. 7, Ecol. Bull.* **22**, 23–73.
Trenberth, K. E., Christy, J. R., and Olson, J. G., 1987, Global atmospheric mass, surface pressure, and water vapor variations, *J. Geophys. Res.* **92**(D12), 14815–14826.
Weiss, R., 1981, The temporal and spatial distribution of tropospheric nitrous oxide, *J. Geophys. Res.* **86**(C8), 7185–7195.
Zeiss, G. D. and Meath, W. J., 1977, Dispersion energy constants $C_6(A, B)$, dipole oscillator strength sums and refractivities for Li, N, O, H_2, N_2, O_2, NH_3, H_2O, NO, and N_2O, *Molec. Phys.* **33**(4), 1155–1176.